Dynamic Analysis of a Cantilever-Mounted Gas-Lubricated Thrust Bearing

I. Etsion
Mem. ASME

I. Green
Department of Mechanical Engineering,
Technion, Haifa, Israel

The dynamic stability of a cantilever-mounted gas-lubricated thrust bearing is analyzed using the step-jump approach. The solution is based on linearization of the equations of motion assuming small perturbation about an equilibrium position. Stiffness and damping of the lubricating film are expressed analytically in terms of Laguerre coefficients thus, enabling a parametric investigation of the bearing. The general theory is used to examine an actual bearing design. It is found that the theoretical results agree with existing experimental data, in that, both show that the bearing is unstable at the design point and becomes more stable as speed decreases.

Introduction

Higher speeds and operating temperatures in modern rotating machinery require bearings that are both stable and have good contaminant ingestion under severe operation conditions. The all-metallic resilient pad gas-lubricated thrust bearing [1] is an example of a bearing concept designed to meet these requirements. In order to optimize the performance of such bearings a theoretical investigation was carried out [2] and as a result the cantilever-mounted gas-lubricated thrust bearing was suggested [3] and analyzed [4]. An experimental bearing, designed to operate at 34,000 rpm, was built and tested successfully up to 17,000 rpm showing good agreement with theoretical predicted performance [5]. However, the design speed of 34,000 rpm could not be reached because of vigorous vibrations in the bearing assembly.

The purpose of this paper is to supplement the steady state analysis [4] with a dynamic investigation of the cantilever-mounted bearing. The step-jump approach [6], which has been previously used in analyzing a gimbal mounted gas lubricated thrust bearing [7], will be applied to determine the effect of various parameters on the stability of the cantilever-mounted bearing.

Following the outlining of the general theory as applicable to the cantilever-mounted gas-lubricated bearing, the particular design of reference [5] will be examined trying to understand its behavior at high speeds.

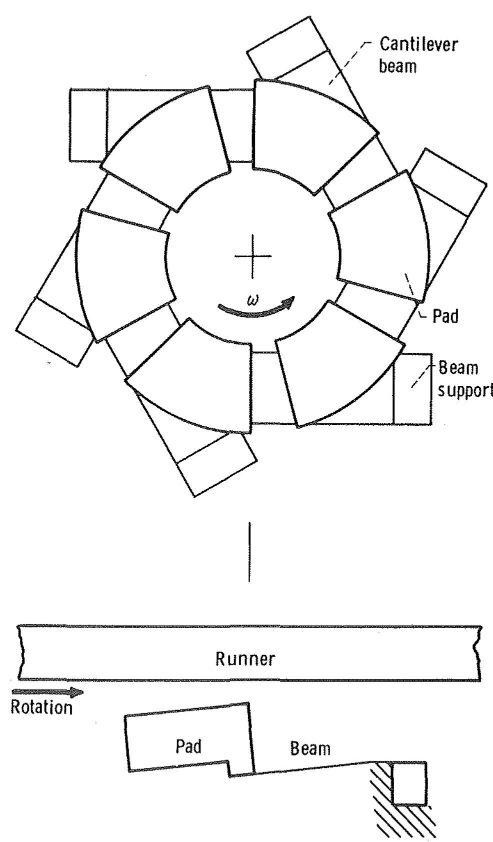

Fig. 1 Schematic of cantilever-mounted thrust bearing

Contributed by the Lubrication Division of THE AMERICAN SOCIETY OF MECHANICAL ENGINEERS and presented at the Century 2 ASME-ASLE International Lubrication Conference, San Francisco, Calif., August 18-21, 1980. Revised manuscript received by the Lubrication Division, February 29, 1980. Paper No. 80-C2/Lub-32.

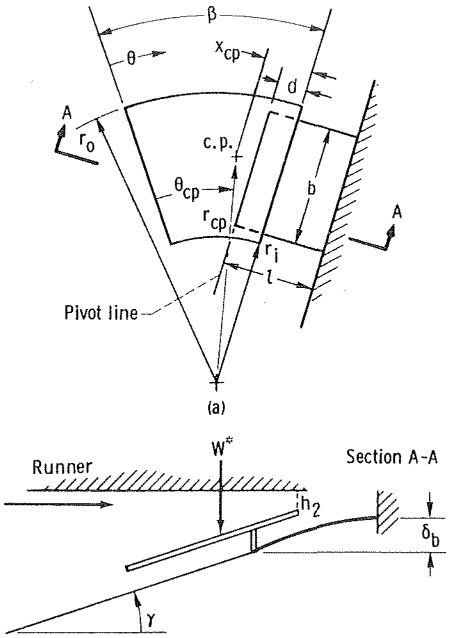

Fig. 2 Details of individual pad

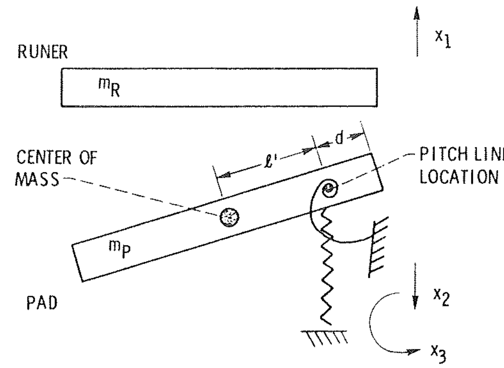

Fig. 3 Model of dynamic system

Bearing Description

Figure 1 is a schematic representation of the cantilever-mounted thrust bearing. The bearing consists of individual sector-shaped flat pads each of which is mounted on a cantilever beam. Beam deflection results in the desired wedge-shape film between runner and pad. The deflection is so designed to allow an optimum pad tilt at selected operating conditions such that the load carrying capacity is a maximum.

Details of an individual cantilever-mounted pad are shown in Fig. 2. The pad is attached to the beam along a line (called the pitch line) that is parallel to the pad trailing edge. This arrangement assures constant minimum film thickness along the trailing edge and hence, maximum load carrying capacity [2]. The pitch angle γ, pitch line location d, and minimum film thickness h_2 completely define the relative position of each pad with respect to the runner as well as the beam end deflection δ_b.

At equilibrium the relations between γ, δ_b, and the load W^* on the pad are found from beam deflection formulas, e.g., [8]. Thus,

$$\delta_b = W^* \frac{l^3}{3EI} + W^*(x_{cp} - d)\frac{l^2}{2EI} \tag{1}$$

$$\gamma = W^* \frac{l^2}{2EI} + W^*(x_{cp} - d)\frac{l}{EI} \tag{2}$$

where W^* $(x_{cp} - d)$ is the moment applied at the beam end by the load W^* acting at x_{cp}, the center of pressure, which is given by

$$x_{cp} = r_{cp} \sin(\beta - \theta_{cp}) \tag{3}$$

A useful relation between γ and δ_b can be found from equations (1) and (2) in the form

$$\frac{\gamma}{\delta_b} = 3\frac{l + 2(x_{cp} - d)}{2l^2 + 3(x_{cp} - d)l} \tag{4}$$

Dynamics of the Cantilever-Mounted Pad

In the following we shall assume that the runner is aligned with the bearing and hence, axisymmetry prevails. In this case, only one pad with its corresponding portion of the runner has to be examined. The dynamic system is shown in Fig. 3 where m_R indicates the rotor mass divided by the number of pads. The runner can move axially thus, it has one degree of freedom designated x_1. The pad can move axially and can also rotate about the pitch line; hence, it has two degrees of freedom x_2 and x_3. However, due to the constraint of the beam these two degrees of freedom are related through equation (4).

The dynamic equations of the bearing can be put into the dimensionless general form

$$M_j \delta \ddot{X}_j(T) = \sum_{i=1}^{3}\left[\delta F_{ij}(T) + \delta B_{ij}(T)\right] \tag{5}$$

where δF_{ij} and δB_{ij} are fluid film and beam forces, respectively, in degree of freedom j responding to a disturbance in degree of freedom i. The beam response can be expressed in

Nomenclature

A_{ijk} = k^{th} Laguerre coefficient for response in j direction due to a jump in i direction
a_{ij} = defined in equation (13)
B_{ij} = dimensionless beam reactions, $b/p_a r_o^2$
b = beam general reaction
C_{ij} = element ij in matrix equation (14)
C_i = ith coefficient in polynomial equation (20)
D = dimensionless pitch line location, d/r_o
d = pitch line location
E = beam modulus of elasticity
G = general mass factor, equation (18)
H_{ij} = dimensionless response in j direction due to a jump in i direction
h = film thickness
h_2 = minimum film thickness
$\bar{h}$ = dimensionless film thickness, h/h_2
I = beam cross section moment of inertia
I_p = pad moment of inertia about pitch line
K_{ij} = beam spring constants (Table 1)
k_L = number of Laguerre coefficients
L = dimensionless length, l/r_o
l = beam length
l' = pad center of mass location
M_j = general dimensionless mass (Table 1)
m_p = pad mass
m_R = rotor mass per pad
N = number of independent degrees of freedom
P = dimensionless pressure, p/p_a
p = pressure
p_a = ambient pressure

terms of spring constants K_{ij} by rearranging equations (1) and (2) in the form

$$\begin{Bmatrix} b_2 \\ \\ b_3 \end{Bmatrix} = \frac{12EI}{l^3}\begin{bmatrix} 1 & -\dfrac{l}{2} \\ \\ -\dfrac{l}{2} & \dfrac{l^2}{3} \end{bmatrix}\begin{Bmatrix} x_2 \\ \\ x_3 \end{Bmatrix} \tag{6}$$

where b_1 and b_2 substitute the force and moment, respectively; and x_2, x_3 replace δ_b and γ, respectively.

Normalizing x_1 and x_2 by h_2, x_3 by h_2/r_o, forces by $p_a r_o^2$, and moments by $p_a r_o^3$ the dimensionless equations of motion are

$$M_1 \delta \ddot{X}_1 = \sum_{i=1}^{3} \delta F_{i1} \tag{7}$$

$$M_2(\delta \ddot{X}_2 + L' \delta \ddot{X}_3) = \sum_{i=1}^{3} \delta F_{i2} + K_{22}\delta X_2 + K_{32}\delta X_3 \tag{8}$$

$$M_3 \delta \ddot{X}_3 + M_2 L' \delta \ddot{X}_2 = \sum_{i=1}^{3} \delta F_{i3} + K_{23}\delta X_2 + K_{33}\delta X_3 \tag{9}$$

In equations (8) and (9) L' is the dimensionless distance l'/r_o (see Fig. 3) from the pad center of mass to the pitch line. The general dynamic forces in equations (8) and (9) are calculated at the pitch line rather than at the pad center of mass. This allows the use of beam reactions at the beam end instead of transforming these reactions to the pad center of mass. The various dimensionless general masses M_j for the jth degree of freedom along with the various spring constants K_{ij} are given in Table 1.

Applying small perturbation about the equilibrium position in each degree of freedom in the form

$$\delta X_i(T) = \delta \bar{X}_i e^{\nu T} \tag{10}$$

and expressing the fluid film general forces $\delta F_{ij}(T)$ in terms of response to step-jump (see Appendix 1) we have

$$\delta F_{ij}(T) = \left[H_{ij}(\infty) + \sum_{k=1}^{\infty} A_{ij}(k-1)\zeta^k \right] \delta \bar{X}_i e^{\nu T} \tag{11}$$

where

$$\zeta = \frac{\nu/\alpha}{\nu/\alpha + 1} \tag{12}$$

Also, denoting

Table 1 Dimensionless Mass M_j and Spring Constants K_{ij}

Degree of freedom j	Dimensionless mass M_j	Dimensionless spring constant K_{ij}		
		$i = 1$	$i = 2$	$i = 3$
1	$\dfrac{m_R h_2 \left(\frac{\omega}{2}\right)^2}{p_a r_o^2}$	0	0	0
2	$\dfrac{m_p h_2 \left(\frac{\omega}{2}\right)^2}{p_a r_o^2}$	0	$-\dfrac{12EIh_2}{p_a r_o^2 l^3}$	$\dfrac{6EIh_2}{p_a r_o^3 l^2}$
3	$\dfrac{I_p h_2 \left(\frac{\omega}{2}\right)^2}{p_a r_o^4}$	0	$\dfrac{6EIh_2}{p_a r_o^3 l^2}$	$-\dfrac{4EIh_2}{p_a r_o^4 l}$

$$a_{ij} = H_{ij}(\infty) + \sum_{k=1}^{\infty} A_{ij}(k-1)\zeta^k \tag{13}$$

equations (7) through (9) can be arranged in a matrix form

$$\begin{bmatrix} C_{11} & C_{21} & C_{31} \\ C_{12} & C_{22} & C_{32} \\ C_{13} & C_{23} & C_{33} \end{bmatrix}\begin{bmatrix} \delta \bar{X}_1 \\ \delta \bar{X}_2 \\ \delta \bar{X}_3 \end{bmatrix} = 0 \tag{14}$$

where the various elements C_{ij} of the matrix are

$$\begin{aligned}
C_{11} &= M_1 \alpha^2 \zeta^2 - (1-\zeta)^2 a_{11} \\
C_{21} &= -(1-\zeta)^2 a_{21} \\
C_{31} &= -(1-\zeta)^2 a_{31} \\
C_{12} &= -(1-\zeta)^2 a_{12} \\
C_{22} &= M_2 \alpha^2 \zeta^2 - (1-\zeta)^2 (a_{22} + K_{22}) \\
C_{32} &= M_2 \alpha^2 \zeta^2 L' - (1-\zeta)^2 (a_{32} + K_{32}) \\
C_{13} &= -(1-\zeta)^2 a_{13} \\
C_{23} &= M_2 \alpha^2 \zeta^2 L' - (1-\zeta)^2 (a_{23} + K_{23}) \\
C_{33} &= M_3 \alpha^2 \zeta^2 - (1-\zeta)^2 (a_{33} + K_{33})
\end{aligned}$$

Recalling that δX_2 and δX_3 are related due to the beam constraint we have

Nomenclature (cont.)

R = dimensionless radius, r/r_o
r = radial coordinate
r_i = pad inner radius
r_o = pad outer radius
T = dimensionless time, $\omega t/2$
t = time
W = dimensionless load $W^*/p_a r_o^2$
W^* = load
X_j = dimensionless coordinate in jth degree of freedom, normalized by h_2 or by h_2/r_o
X_{cp} = dimensionless distance x_{cp}/r_o
x_j = general coordinate in jth degree of freedom
x_{cp} = center of pressure location
α = attenuation coefficient
β = sector angle
γ = tilt angle about pitch line, beam angular deflection
δ_b = beam end deflection
δF_{ij} = dimensionless fluid film force in j direction due to a jump in i direction
δX_j = dimensionless displacement in jth degree of freedom
ΔX_j = dimensionless step-jump in jth degree of freedom
ϵ = tilt parameter, $\gamma r_o/h_2$
ζ = transform variable, equation (34)
θ = angular coordinate
λ = beam constraint factor, equation (16)
Λ = compressibility number, $6\mu\omega r_o^2/p_a h_2^2$
μ = gas viscosity
ν = complex exponent
ω = shaft angular velocity

Subscripts

cp = center of pressure
eq = equilibrium
o = old
n = new

$$\delta\bar{X}_3 = \lambda\delta\bar{X}_2 \quad (15)$$

where by equation (4)

$$\lambda = \frac{L + 2(X_{cp} - D)}{\frac{2}{3}L^2 + (X_{cp} - D)L} \quad (16)$$

The dimensionless mass M_3 (see Table 1) is a measure of the pad moment of inertia about the pitch line, which, for a pad of uniform thickness, relates to the mass m_p by

$$I_p = \frac{1}{4}m_p r_o^2\left[1 + \left(\frac{r_i}{r_o}\right)^2\right]\left(1 - \frac{\sin 2\beta}{2\beta}\right) - m_p(d - 2l')$$

Hence, multiplying by $h_2(\omega/2)^2/p_a r_o^4$ we have

$$M_3 = GM_2 \quad (17)$$

where

$$G = \frac{1}{4}\left[1 + \left(\frac{r_i}{r_o}\right)^2\right]\left(1 - \frac{\sin 2\beta}{2\beta}\right) - D^2\left(1 + 2\frac{l'}{d}\right) \quad (18)$$

Using equations (15) and (17) in (14), and combining the second and third rows of the matrix we finally have

$$\begin{bmatrix} C_{11} & C_{21} + \lambda C_{31} \\ C_{12} + C_{13} & C_{22} + C_{23} + \lambda(C_{32} + C'_{33}) \end{bmatrix}\begin{bmatrix} \delta\bar{X}_1 \\ \delta\bar{X}_2 \end{bmatrix} = 0 \quad (19)$$

where

$$C'_{33} = GM_2\alpha^2\zeta^2 - (1-\zeta)^2(a_{33} + K_{33})$$

For a solution of (19) to exist the determinant of the coefficient matrix must equal zero. Each element of this determinant is a series in ζ, hence the expansion of the determinant yields a polynomial in ζ of order $N(k_L + 2)$

$$C_o + C_1\zeta + C_2\zeta^2 + \ldots C_{N(k_L+2)}\zeta^{N(k_L+2)} = 0 \quad (20)$$

where N is the number of independent degrees of freedom (two in our case), and k_L is the finite number of Laguerre coefficients A_{ijk} needed in equation (11).

Equation (20) represents the characteristic equation of the dynamic system shown in Fig. 3. The roots of ζ are transformed to values of ν by equation (12). If any of the real parts of ν is greater than zero, then the system is unstable for that particular set of dynamic parameters.

Results and Discussion

The general theory described in the previous section was used to analyze the effect of beam geometry and pad and runners masses on the stability of the cantilever-mounted bearing described in reference [5]. The bearing has the following dimensions and operating conditions:

Outer radius, r_o, m	5×10^{-2}
Inner radius, r_i, m	2.5×10^{-2}
Ambient pressure, p_a, N/m^2	10^5
Dynamic viscosity of gas (air), μ, Ns/m^2	1.86×10^{-5}
Angular velocity, ω, rpm	34.000
Total load, W^*, N	74
Young modulus of beam material, $E, N/m^2$	2.1×10^{11}

The bearing consists of six individual pads; hence, the load per pad is 74/6 N. In reference [4] it was found that this bearing will operate optimally if the compressibility number is $\Lambda = 50$ and the tilt parameter is $\epsilon = 3.2$, where

$$\Lambda = 6\mu\omega r_o^2/p_a h_2^2$$

and

$$\epsilon = \gamma r_o/h_2$$

Table 2 Laguerre Coefficients

k	A_{11k}	A_{13k}	A_{31k}	A_{33k}
0	−0.00872	−0.00338	−0.02325	−0.00550
1	−0.00397	−0.00226	−0.00924	−0.00269
2	−0.00159	−0.00157	−0.00304	−0.00133
3	−0.00055	−0.00114	−0.00068	−0.00072
4	−0.00022	−0.00087	−0.00005	−0.00047
5	−0.00023	−0.00071	−0.00004	−0.00036

The first step in the analysis is to obtain a steady state solution for the pressure distribution in the lubricating film. This can be done by solving the Reynolds equation using one of the methods described in [9]. It is very important that the numerical results be as accurate as possible to avoid large errors in computing the response coefficients H_{ij} (see Appendix 1). Hence, if using an iterative solution for the pressure, the convergence criterion should be very small. In the present work a criterion of 10^{-7} was used to determine pressure convergence [10]. Such an accuracy was achieved by first solving for $(P\bar{h})^2$ using successive over-relaxation technique to get fast initial convergence, and then letting the pressure diffuse with time until the difference in grid pressures over successive time iterations became less than 10^{-7}.

The step-jumps for calculating H_{ij} (see Appendix 1) were $\Delta X_1 = \Delta X_2 = 0.02$ and $\Delta X_3 = 0.03$. These jumps correspond to 2 percent of the equilibrium dimensionless minimum film thickness and about 1 percent of the equilibrium tilt. Various time steps were examined [10] and it was found that with $\Delta T = 10^{-2}$ one hundred time steps are enough to obtain the asymptotic values $H_{ij}(\infty)$. However, a time step $\Delta T = 2\times10^{-3}$ was used in order to get more data points for $H_{ij}(T)$ and hence better accuracy in fitting the Laguerre polynomials to the numerical results. Examination of various values of attenuation coefficient α revealed that $\alpha = 3.8$ resulted in the fastest convergence of the series of Laguerre coefficients A_{ijk}. These coefficients are presented in Table 2 from which it is seen that 6 terms are sufficient for the series of A_{ijk}.

Once the response coefficients at the new equilibrium position $H_{ij}(\infty)$ and the Laguerre coefficients A_{ijk} are known a parametric investigation of the bearing stability can be performed. The computer program is described in detail in [10]. Basically, it calculates for a given set of pad geometry and operating conditions, and for various values of L, D, M_1, and M_2 the following:

(1) Center of mass location L' (see Fig. 3)

(2) The factors λ and G (equations (16) and (18))

(3) Spring constants K_{ij}. Here only K_{22} is needed (see Appendix 2) since all the other constants can be expressed in terms of K_{22}

(4) The coefficients C_i of the polynomial equation (20)

(5) The roots ζ_i of the polynomial equation (20) and their corresponding ν_i (equation (12))

Finally, the program searches for the value of M_2 which makes the largest real part of all ν_i zero for a set of parameters M_1, L, and D, thus finding the stability threshold for the bearing.

The bearing of [5] was designed with a beam length $L = 0.8$ and pitch location $D = 0$. The rotor dimensionless mass per

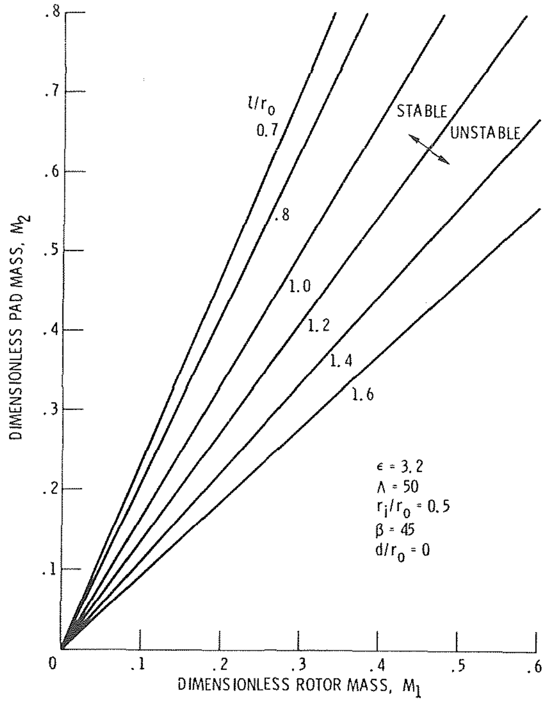

Fig. 4 Stability map for $D = 0$

pad and the pad mass were $M_1 = 0.225$, and $M_2 = 7.1 \times 10^{-2}$, respectively. Hence, the range of the various parameters for the present investigation was $0.6 \leq L \leq 1.6$, $0 \leq D \leq 0.35$, $0.1 \leq M_1 \leq 0.6$, and $10^{-4} \leq M_2 \leq 10$. A too long or too short beam is impractical because of space limitations (see Fig. 1).

Figure 4 is an example of a stability map for the case $D = 0$ and various beam lengths L. An interesting result is the linear relation between M_1 and M_2 at stability threshold. For any given value L the ratio M_2/M_1 is a constant depending only on L. This result is typical of all the pitch line locations D examined in this work. Similar results were obtained in [7] where a linear relation was found between the moments of inertia of inner and outer gimbals of the gimbal-mounted bearing.

The result of constant values for the ratio M_2/M_1 at any D and L enables one to plot these constant values at the stability threshold as functions of the dimensionless beam length and pitch line location. Fig. 5 presents stability maps obtained from such plots. No data is shown in the figure for $L < 2D$ since it was found in [4] that $L \geq 2D$ is necessary for proper operation. Both M_1 and M_2 are linearized by the same factor, hence the ratio M_2/M_1 is identical to the ratio m_p/m_R. It is clear from Fig. 5 that at any given ratio m_p/m_R the bearing stability is improved by increasing l/r_0 and d/r_0. Increasing both l/r_0 and d/r_0 without increasing the housing size can be accomplished by holding the beam support at its place and moving the pitch line toward the pad leading edge (see Figs. 1 and 2).

The bearing of reference [5] has a mass ratio of $m_p/m_R = 0.0315$, beam length $l/r_0 = 0.8$, and pitch line location $d/r_0 = 0$. As can be seen from Fig. 5 such bearing is very unstable at the given load and speed of the design point. Indeed, the bearing in [5] operated well only up to 17,000 rpm where vigorous vibration started and prevented further increase in speed.

As an attempt to study the effect of shaft speed ω on the stability of the bearing described in [5], two slightly off-design points were also examined. These were at $\Lambda = 50$ and $D = 0$ but at tilt parameter values $\epsilon = 3.6$ and $\epsilon = 2.8$ (the tilt parameter at the design point is 3.2). A higher ϵ value in-

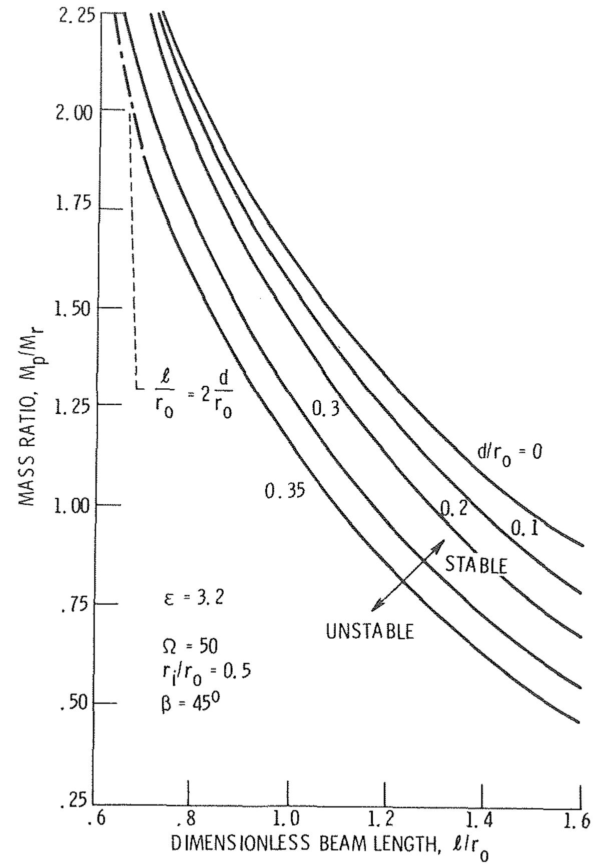

Fig. 5 Thrust bearing stability as a function of beam length and pitch line location, $\epsilon = 3.2$

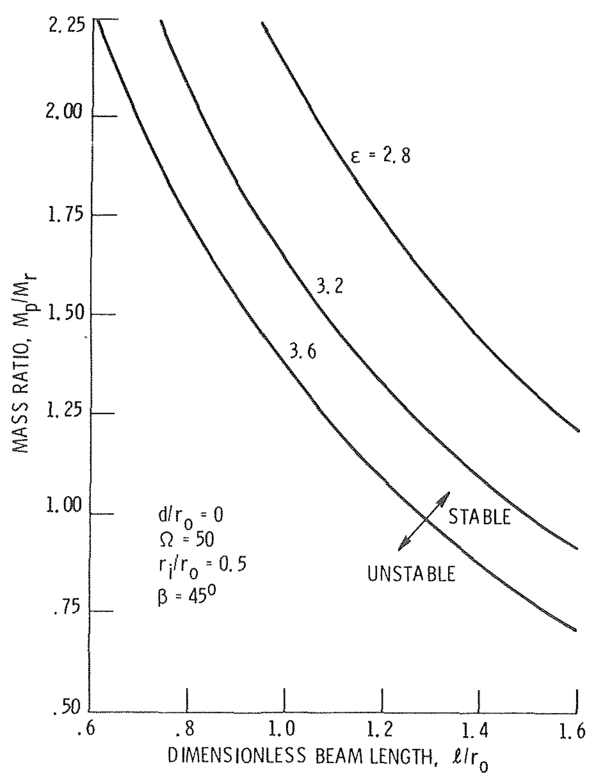

Fig. 6 Thrust bearing stability as a function of beam length and tilt parameter, $d/r_0 = 0$

dicates lower shaft speed since the minimum film thickness decreases with decreasing speed. The results are presented in Fig. 6. It is clear from the figure that the bearing tends to become more stable as the speed decreases. This result fairly agrees with the general trend found experimentally in [5].

As can be seen from Fig. 5 the bearing of reference [5] with the mass ratio $m_p/m_R = 0.0315$ could not be stabilized at the design point with any practical beam geometry. Changing the mass ratio would not help either since the ratios needed are too high and impractical. Hence, it seems as if the best way to improve stability is by providing more damping to the system. This can be done, for example, by adding external Coulamb friction on the sides of the beams. The present analysis does not include damping other than this presented by the Laguerre coefficients. Further investigation is needed to determine how much damping is required to stabilize the bearing.

Conclusion

The step-jump approach is implied to a parametric investigation of a cantilever-mounted gas-lubricated thrust bearing dynamics. The general theory is presented and then used to examine an actual bearing design. The bearing was found unstable at its design point of 34,000 rpm both experimentally and by the theoretical analysis presented here. The theory indicates improvement in stability as speed decreases. Experimental results show stable operation at 17,000 rpm. It is suggested that bearing stability at the design point could be improved by adding damping to the system. Further investigation is needed to determine how much damping is required to stabilize the bearing.

References

1 Anderson, W. J., "Analysis of an All-Metallic Resilient Pad Gas-Lubricated Thrust Bearing," ASME JOURNAL OF LUBRICATION TECHNOLOGY, Vol. 97, No. 2, Apr. 1975, pp. 296–302.

2 Etsion, I., and Fleming, D. P., "An Accurate Solution of the Gas Lubricated, Flat Sector Thrust Bearing," ASME JOURNAL OF LUBRICATION TECHNOLOGY, Vol. 99, No. 1, Jan. 1977, pp. 82–88.

3 Etsion, I., "A Cantilever Mounted Resilient Pad Gas Bearing," U.S. Patent 4,099, 799, July 11, 1978.

4 Etsion, I., "A Cantilever Mounted Resilient Pad Gas Thrust Bearing," ASME JOURNAL OF LUBRICATION TECHNOLOGY, Vol. 99, No. 1, Jan. 1977, pp. 95–100.

5 Nemeth, Z. N., "Operating Characteristics of a Cantilever Mounted Resilient-Pad Gas-Lubricated Thrust Bearing," NASA TP-1438, 1979.

6 Elrod, H. G., McCabe, J. T., and Chu, T. Y., "Determination of Gas Bearing Stability by Response to a Step-Jump," ASME JOURNAL OF LUBRICATION TECHNOLOGY, Vol. 89, No. 4, Oct. 1967, pp. 493–498.

7 Shapiro, W., and Colsher, R., "Implementation of Time-Transient and Step-Jump Dynamic Analyses of Gas Lubricated Bearings," ASME JOURNAL OF LUBRICATION TECHNOLOGY, Vol. 92, No. 3, July 1970, pp. 518–529.

8 Roark, R. J., *Formulas for Stress and Strain,* McGraw-Hill, 1965.

9 Castelli, V., and Privics, J., "Review of Numerical Methods in Gas Bearing Film Analysis," ASME JOURNAL OF LUBRICATION TECHNOLOGY, Vol. 90, No. 4, Oct. 1968, pp. 777–792.

10 Green, I., "Dynamic Analysis of Flexibly Mounted Gas Thrust Bearing," M.Sc. thesis, Technion-Israel Institute of Technology, Aug. 1979.

11 Churchill, R. V., *Modern Operational Mathematics in Engineering,* McGraw-Hill, New York, 1944.

APPENDIX 1

Step-Jump Approach as Applied to the Cantilever-Mounted Bearing

The method assumes the bearing is in an equilibrium position and then obtains responses to a small disturbance by using of small perturbation techniques. Suitable polynomial representation of the responses permits a characteristic equation to be established and hence, a parametric investigation of the system. The general procedure is as follows:

(*a*) For a given operation condition (Λ,ϵ) obtain a steady state solution of the Reynolds equation

$$\frac{\partial}{\partial R}\left(RP\bar{h}^3\frac{\partial P}{\partial R}\right)+\frac{1}{R}\frac{\partial}{\partial\theta}\left(P\bar{h}^3\frac{\partial P}{\partial\theta}\right)=\Lambda R\left[\frac{\partial(P\bar{h})}{\partial\theta}+\frac{\partial(P\bar{h})}{\partial T}\right] \tag{21}$$

where for the particular bearing

$$\bar{h}=1+\epsilon R\ \sin(\beta-\theta)$$

For the steady state solution $\partial(P\bar{h})/\partial T$ in (21) is set equal to zero. After the pressure P is found the load at equilibrium, W_{eq}, and center of pressure, X_{cp}, are calculated by integrations of P over the pad area.

(*b*) The bearing is given a step jump in one of its degrees of freedom and the new film thickness distribution $\bar{h}_n$ is computed. If the jump is in one of the translational degrees of freedom X_1 or X_2, the new film thickness will be $\bar{h}_n = \bar{h}_o + \Delta X$. If, however, the jump is in the rotational degree of freedom we have

$$\bar{h}_n=1+(\epsilon+\Delta X_3)R\ \sin(\beta-\theta) \tag{22}$$

In the second case there is no change in the minimum film thickness; hence, the compressibility number Λ does not change. However, with the jumps ΔX_1 or ΔX_2 the minimum film thickness changes and the new compressibility number becomes

$$\Lambda_n=\frac{6\mu\omega r_o^2}{p_a(h_2+\Delta h_2)^2}=\frac{\Lambda_o}{(1+\Delta X)^2}$$

(*c*) Since the jump is an isothermal process, the value of $P\bar{h}$ remains constant. Therefore, after the jump, pressures throughout the grid of the pad area are computed from

$$P_n=P_o\frac{\bar{h}_o}{\bar{h}_n} \tag{23}$$

(*d*) With the new values of pressures, the new load and center of pressure at time $T = 0$ are computed. The calculation is then repeated at a time $T + \Delta T$ by using the known pressures from the previous time T in equation (21) along with the film thickness distribution $\bar{h}_n$ and the compressibility number Λ_n. Thus,

$$P(T+\Delta T)=P(T)+\frac{dP}{dT}(T)\Delta T \tag{24}$$

The load and center of pressure values of each time step are saved, and the procedure is continued forward in time until a new steady state condition is reached. Dimensionless responses are computed from the following:

$$H_{11}(T)=\frac{W(T)-W_{eq}}{\Delta X_1} \tag{25}$$

$$H_{13}(T)=\frac{W(T)\left[x_{cp}(T)-D\right]-W_{eq}(X_{cp,eq}-D)}{\Delta X_1} \tag{26}$$

$$H_{31}(T)=\frac{W(T)-W_{eq}}{\Delta X_3} \tag{27}$$

$$H_{33}=\frac{W(T)\left[x_{cp}(T)-D\right]-W_{eq}(X_{cp,eq}-D)}{\Delta X_3} \tag{28}$$

From Fig. 3 we can see that

$$H_{22}(T)=H_{21}(T)=H_{12}(T)=H_{11}(T)$$
$$H_{23}(T)=H_{13}(T)$$
$$H_{32}(T)=H_{31}(T)$$

hence, only the four responses H_{11}, H_{13}, H_{31}, and H_{33} are needed to determine the total of nine responses H_{ij}.

The numerical data of H_{ij} is best fitted by Laguerre polynomials [6] in the form

$$H_{ij}(T) = H_{ij}(\infty) + \sum_{k=0}^{\infty} A_{ijk} L_k(\alpha T) e^{-\alpha T} \tag{29}$$

where $H(\infty)$ is the response after the new equilibrium is reached, and α is an attenuation factor. The Laguerre coefficients A_{ijk} in (29) are determined from

$$A_{ijk} = \alpha \int_0^\infty \Big[H_{ij}(T) - H_{ij}(\infty) \Big] L_k(\alpha T)\, dT \tag{30}$$

where

$$L_k(\xi) = \sum_{m=0}^{k} \frac{k!}{(k-m)!\ m!} \frac{(-\xi)^m}{m!} \tag{31}$$

The two unknowns in (30) are the number of terms, k_L, necessary for convergence of the series, and the value of the attenuation coefficient α. Selecting an optimum value for α results in fast convergence of the Laguerre coefficients A_{ijk} and, hence, a small number of terms k_L. Selection of optimal α is accomplished by curve fitting routines through trial and error until the desired fit of the numerical data for H_{ij} (T) is achieved.

The deviational fluid film forces can be expressed [6] in the general form

$$\delta F_{ij}(T) = H_{ij}(\infty) \delta X_i(T) + \int_0^T \delta \dot{X}_i(T-\tau) \sum_{K=0}^{\infty} A_{ijk} L_k(\alpha\tau) e^{-\alpha\tau} d\tau \tag{32}$$

Substituting equation (10) in (32) we obtain

$$\delta F_{ij}(T) = \left[H_{ij}(\infty) + \frac{\nu}{\alpha} \sum_{k=0}^{\infty} A_{ijk} \int_0^T L_k(\alpha\tau) e^{-\left(\frac{\nu}{\alpha}+1\right)\alpha\tau} d(\alpha\tau) \right] \delta\bar{X} e^{\nu T} \tag{33}$$

As $T \to \infty$, which is the case for examining asymptotic stability, the integral in (33) becomes a Laplace transform. Defining

$$\psi = \alpha\tau$$

and

$$\zeta = \frac{\nu/\alpha}{\nu/\alpha + 1} \tag{34}$$

The Laplace transform has the form

$$\int_0^\infty L_k(\psi) e^{-\left(\frac{\nu}{\alpha}+1\right)\psi} d\psi = \frac{\alpha}{\nu} \zeta^{k+1} \tag{35}$$

Substituting equation (35) in equation (33) we finally obtain equation (11).

APPENDIX 2

Spring Constants of the Cantilever Beam

As can be seen from Table 1 spring constants K_{ij} can be expressed in terms of K_{22} in the form

$$K_{23} = K_{32} = -\frac{1}{2} \frac{l}{r_o} K_{22}$$

$$K_{33} = \frac{1}{3} \left(\frac{l}{r_o} \right)^2 K_{22}$$

The constant K_{22} itself is obtained from matching the beam deflection with the required pad tilt at the design point. Thus, from equation (2)

$$EI = \frac{W^* l^2}{2\gamma} \left(1 + 2 \frac{x_{cp} - d}{l} \right) \tag{36}$$

Using the definitions $\epsilon = \gamma r_o / h$, $W = W^* / p_a r_o^2$, and the expression for K_{22} given in Table 1 we have from (36)

$$K_{22} = -6 \frac{W_{eq}}{\epsilon} \frac{1}{L} \left(1 + 2 \frac{X_{cp,eq} - D}{L} \right) \tag{37}$$

Hence, for a given design point (W_{eq}, ϵ, $X_{cp,eq}$) the spring constant K_{22}, and by it all the other constants K_{ij} are determined by the selection of L and D for the supporting beam.

From equation (37) and the definition of K_{22} in Table 1 it is clear that the beam cross section moment of inertia I is not an independent variable. Once L and D are selected I is determined by these two parameters, by the design point conditions (W_{eq}, ϵ, $X_{cp,eq}$), and by the modulus of elasticity, E, of the beam material.